Traveling waves support rhythmic attentional search

Yue Kong[1,*], Kirsten Petras[1], Philippe Marque[2,3], Rufin VanRullen[4], David M. Alexander[1,#], Laura Dugué[1,5,#]

Affiliations

[1]Université Paris Cité, CNRS, Integrative Neuroscience and Cognition Center, F-75006 Paris, France

[2]Department of Physical and Rehabilitation Medicine, University Hospital of Toulouse, Toulouse, France

[3]ToNIC (Toulouse NeuroImaging Center), Inserm, University of Toulouse 3, Toulouse, France

[4]CerCo, CNRS, Universite de Toulouse, Toulouse, France

[5]Institut Universitaire de France (IUF), Paris, France

*Correspondence: yue.kong@u-paris.fr

[#]Shared senior authorship

Abstract

Brain activity unfolds across space and time, giving rise to spatiotemporal dynamics that can manifest as cortical traveling waves –smooth phase shifts propagating across the cortex. Although traveling waves have been observed across species and measurement scales, their functional role in human cognition remains largely inferred from correlational evidence. In healthy humans, large-scale neural dynamics must be studied non-invasively, which provides limited access to their neural origins. Here, we tested whether global traveling waves causally contribute to inter-areal communication during attention. Using transcranial magnetic stimulation (TMS), we induced long-range traveling waves detectable with electroencephalography and assessed their neural and behavioral consequences during an attentional search task. Double-pulse TMS applied over the right frontal eye field transiently disrupted ongoing global waves and selectively induced direction- and frequency-specific traveling waves propagating toward the occipital visual cortex. These TMS-induced anterior-to-posterior theta traveling waves were rhythmically modulated by stimulation latency relative to search-trial onset. Critically, behavioral performance exhibited the same rhythmic pattern, with improved attentional search performance when TMS-induced traveling waves were more prominent. Together, these findings provide causal evidence that large-scale traveling waves support inter-areal communication during rhythmic visual attention.

Introduction

Traveling waves –smooth phase shifts across the cortex (Muller et al., 2018; Dugué & Chavane, 2025)– have been observed across species and scales and have been linked to cognitive processes (Zhang et al., 2018; Lozano-Soldevilla & VanRullen, 2019; Davis et al., 2020; Alamia et al., 2023; Fakche & Dugué, 2024; Fakche et al., 2024). In humans, electro- or magneto-encephalography (EEG, MEG) studies have reported wave-like patterns across the sensor array, but the significance of these observations is debated, partly due to uncertainties regarding their computational underpinnings (Grabot et al., 2025; Petras et al., 2025; Dugué & Chavane, 2025). This raises concerns about the functional relevance of these large-scale, non-invasively measured traveling waves. Here, we address this issue by using transcranial magnetic stimulation (TMS) to causally induce global traveling waves in EEG signals and examine their behavioral consequences.

Cortical traveling waves have been proposed as a canonical computation that organizes neuronal processing across space and time in a variety of cognitive functions, including attention (Dugué & Chavane, 2025). Attention itself is intrinsically spatiotemporal, and samples multiple objects in the sensory environment across space and time in a rhythmic manner, as reflected in theta-frequency (4-7 Hz) fluctuations in behavioral performance (VanRullen et al., 2007; Landau & Fries, 2012; Fiebelkorn et al., 2013; Senoussi et al., 2019; Galas et al., 2025; for review: Dugué & VanRullen, 2017; Fiebelkorn & Kastner, 2019; Kienitz et al., 2022). Such rhythmic modulations of performance can similarly be induced by time-locked perturbations such as with TMS. For example, when TMS is applied at different latencies relative to task events over the right frontal eye field (rFEF), a key region of the attention network (Corbetta & Shulman, 2002; Corbetta et al., 2008; Scolari et al., 2015), visual attentional performance is periodically modulated over time (Dugué et al., 2019; Veniero et al., 2021). The rhythmic nature of visual attention aligns with neuroimaging evidence linking it to local, stationary neural oscillations in frontal (e.g., rFEF, Helfrich et al., 2018; Fiebelkorn et al., 2018) and occipital regions (Dugué et al., 2015; Landau et al., 2015; Plöchl et al., 2022). The involvement of both

frontal and occipital regions is consistent with two-stage models of attention in which inter-areal iterative communication between low-level sensory processing regions and higher-order attention regions mediates attentional search (Palmer et al., 1993; Treisman, 1998; Itti & Koch, 2001; Deco et al., 2002). Yet, the neural mechanisms supporting such long-range coordination remain unclear.

Here, we investigate whether global traveling waves support inter-areal communication in visual attention. We tested the hypothesis that anterior-to-posterior global theta traveling waves have a causal, functional role in attentional search. We applied double-pulse TMS over rFEF (or over the vertex as a control site) at multiple stimulation latencies in an attentional search task while simultaneously recording EEG. TMS perturbed ongoing wave dynamics and selectively induced direction- and frequency-specific traveling waves. These TMS-induced traveling waves were rhythmically modulated by TMS latency, and this modulation correlated with rhythmic fluctuations in attentional search performance induced by TMS, thereby directly linking traveling wave dynamics to behavioral outcomes. Taken together, our results show that TMS-induced global traveling waves support inter-areal communication in rhythmic attentional search.

Results

We tested the hypothesis that anterior-to-posterior global theta traveling waves have a causal functional role in attentional search. Participants performed an attentional search task with concurrent EEG recordings (Fig. 1a). Double-pulse TMS was applied over the rFEF at various latencies from search array onset. Stimulation of the vertex served as a control condition (Fig. 1b). We characterized global traveling wave activity in sensor space using a data-driven approach, complemented by time-frequency analyses and permutation-based statistical testing (Fig. 1c). We first assessed the prevalence of global traveling waves in TMS–EEG recordings, then examined how TMS transiently disrupted ongoing wave activity while inducing frequency- and direction-specific traveling waves. We then tested whether these TMS-induced

waves were rhythmically modulated as a function of TMS latency. Finally, we compared this rhythmic modulation of TMS-induced traveling waves to rhythmic fluctuations in attentional search performance, such that more TMS-induced waves are correlated with improved behavioral outcome. Note that the behavioral effect observed in this experiment, i.e., rhythmic attentional performance, was previously reported in Dugué et al. (2019).

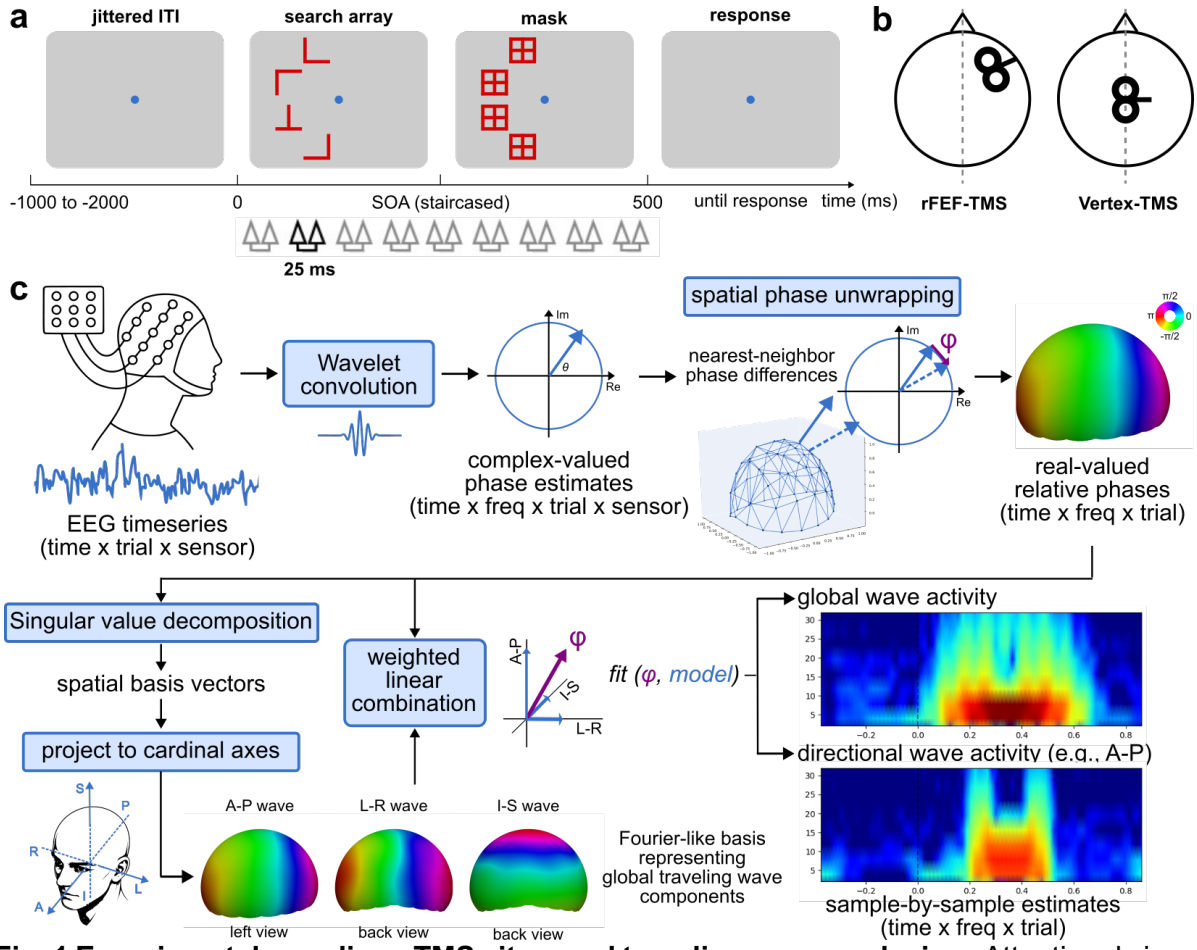

Fig. 1 Experimental paradigm, TMS sites, and traveling wave analysis. a Attentional visual search task. Each trial began with a 1000-2000 ms jittered inter-trial interval (ITI). A four-item search array was briefly presented in the left visual field and masked after a staircase-determined stimulus-onset asynchrony (SOA), such that total visual stimulation lasted 500 ms. Participants reported the presence or absence of target "T" among distractor "L"s. A double-pulse TMS (25 ms inter-pulse interval) was delivered at one of nine delays during stimulus presentation. **b** TMS pulses were applied over the rFEF (left) or the vertex (right) as a control site. **c** Traveling wave analysis pipeline. Single-trial EEG data were wavelet-transformed to obtain complex-valued phase estimates, and then spatially unwrapped (via nearest-neighbor phase differences) into real-valued relative phases referenced to an arbitrary electrode (see Methods section). Singular value decomposition (SVD) was applied to the relative phases to extract spatial basis vectors. The first four spatial basis vectors were projected onto interpretable Cartesian dimensions of sensor space, yielding anterior-posterior (A-P), left-right (L-R), and inferior-superior (I-S) global traveling wave components. Relative phases were then reconstructed as a weighted linear combination of these components, providing sample-by-sample estimates of global or direction-specific wave activity across time and frequency (time-frequency wave maps).

Theta-band power is selectively enhanced following TMS

To demonstrate the frequency specificity and the power of TMS-induced activity, we examined time-frequency representations and topographical distributions of induced power within trials in which TMS was applied at the latest latency (450 ms after search array onset). Grand-average power, computed across trials and sensors, revealed significant increases in the theta band (4.76-5.66 Hz) at two distinct post-stimulus intervals: an early window around 104-204 ms and a later window around 436-536 ms following search array onset (Fig. 2a and 2b). These time-frequency windows corresponded to visually-induced and TMS-induced activity, respectively, as confirmed by their corresponding scalp topographies (Fig. 2c). Theta power peaked over right occipital electrodes during the early window (104-204 ms) in both rFEF-TMS and Vertex-TMS conditions, consistent with visual stimulation in the left visual field. During the later window (436-536 ms), right frontal power peaked in the rFEF-TMS condition, whereas power increases in the Vertex-TMS condition were localized near electrode Cz and did not reach statistical significance (Fig. 2c; permutation tests, see Methods section).

Importantly, the visually-induced theta cluster fell outside the time-frequency cone of influence surrounding the TMS pulses confirming that it is not an artifact of the wavelet convolution. This cluster showed a clear temporal separation between visually-induced and TMS-induced activity; indicating the high temporal resolution of our time-frequency decomposition. Consistent with this interpretation, only the TMS-induced activity exhibited systematic temporal shifts across TMS latencies, whereas visually-induced theta power remained stable in both timing and magnitude across TMS latencies and stimulation conditions (Supplementary Fig. S1).

Direct comparison between conditions using cluster-based permutation testing further demonstrated significantly greater low-frequency power in the rFEF-TMS condition relative to the Vertex-TMS condition. These results suggest that TMS preferentially enhances theta-band

activity, particularly following rFEF stimulation, providing a frequency-specific context for the subsequent observation of TMS-induced theta traveling waves.

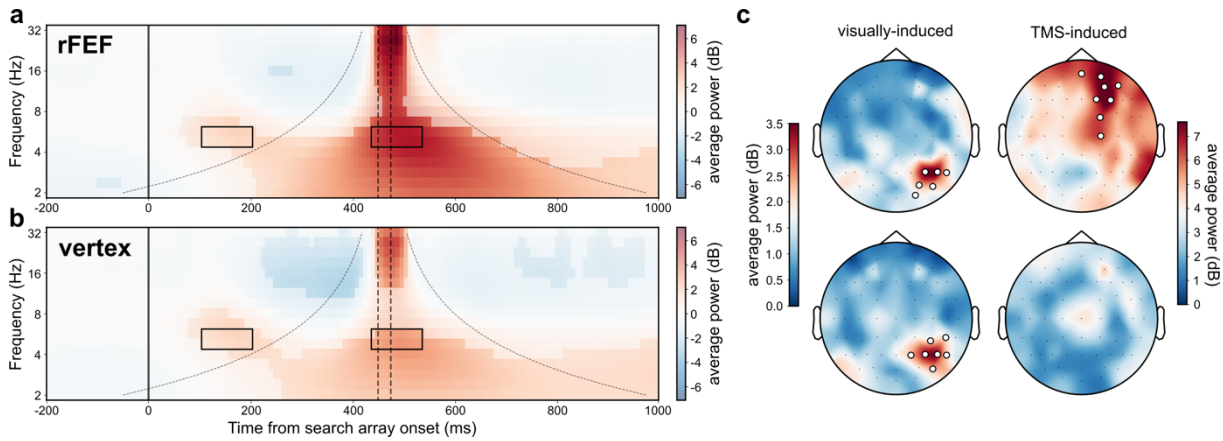

Fig. 2 Theta-band power is selectively enhanced following TMS. a Grand-average time-frequency power (across trials and sensors) in the rFEF-TMS condition. The solid black line marks search array onset; dashed vertical lines indicate TMS single-pulse onsets. The cone of influence is overlayed (area potentially impacted by artifactual spread of the TMS-induced activity). Non-transparent regions denote significant clusters identified by permutation testing. **b** Same as **a**, but for the Vertex-TMS (control) condition. **c** Scalp topographies averaged over the time-frequency windows outlined by black boxes in **a** (top row) and **b** (bottom row). Left column shows visually-induced activity averaged over 104-204 ms; right column shows TMS-induced activity averaged over 436-536 ms. Black circles outline electrodes within clusters of significant positive difference to zero (permutation testing).

Global traveling waves dominate EEG dynamics

Before testing our hypothesis that anterior-to-posterior global theta traveling waves have a causal functional role in attentional search, we first confirm that global traveling waves constitute a dominant component of EEG dynamics in the context of concurrent TMS-EEG experiments. To this end, global traveling wave components were empirically extracted for each participant using a singular-value-decomposition (SVD)-based approach (see Methods section). We define global traveling waves as phase dynamics with a spatial frequency of one cycle across the entire electrode array.

Across participants, the first four spatial basis vectors (main phase patterns; Fig. 1c) explaining the largest proportion of variance consistently exhibited a low spatial frequency, corresponding to approximately one cycle across the measurement array. Subsequent spatial basis vectors showed higher spatial frequencies and explained substantially less variance. By projecting these low-frequency spatial basis vectors onto three interpretable cardinal axes, we identified

three global traveling wave components propagating along the anterior-posterior, inferior-superior, and left-right directions (Fig. 3a; see examples in Supplementary Fig. S2).

The proportion of variance explained by each component is shown in Fig. 3b. The anterior-posterior component accounted for the largest share of variance, followed by the left-right component and the inferior-superior component. Low spatial-frequency global traveling waves account for the majority of EEG variance (58.13-69.76 %) and thus dominate cortical dynamics during concurrent TMS-EEG recordings. Notably, the summed variance explained by these three axes slightly exceeded 100 %, as the projection procedure renders the components marginally non-orthogonal.

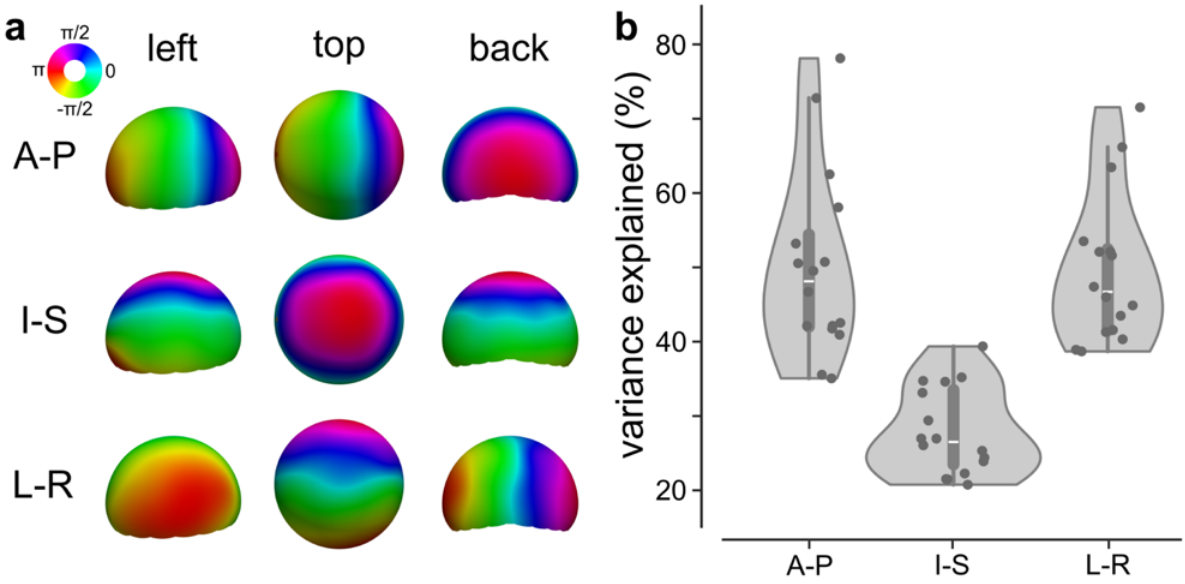

Fig. 3 Global traveling waves dominate EEG dynamics. a Global traveling wave components projected onto cardinal axes (collapsed for participants). **b** Variance explained by each global traveling wave component after cardinal transformation across individual participants. A-P: anterior-posterior; I-S: inferior-superior; L-R: left-right.

TMS transiently disrupts global wave activity

To assess the effect of TMS on ongoing traveling waves, trials were realigned to TMS onset, and global wave activity –defined as the fit of the model wave to real-valued phases (relative to an arbitrary electrode)– was computed as a function of time and frequency. Permutation testing revealed a significant transient reduction in global wave activity time-locked to TMS onset in both the rFEF-TMS (Fig. 4a) and Vertex-TMS conditions (Fig. 4b). This disruption was

temporally specific to the TMS pulses, as evidenced by its systematic temporal shift across different TMS latencies (Supplementary Fig. S3), indicating that the observed effect reflects TMS-induced disruption of ongoing wave dynamics rather than task-related or spontaneous fluctuations.

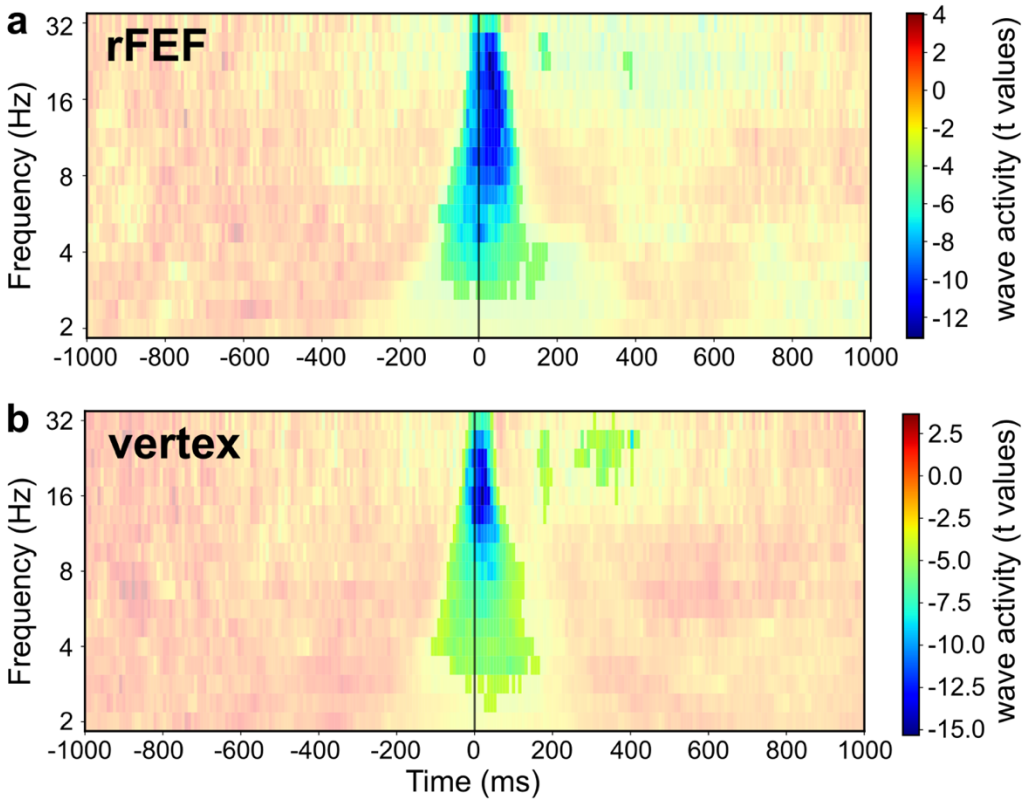

Fig. 4 TMS transiently disrupts global wave activity. a Global traveling wave activity (t values) across time and frequency in the rFEF-TMS condition. The solid black line marks TMS onset (first pulse). Non-transparent regions indicate significant clusters identified by permutation testing. **b** Same as **a**, but for the Vertex-TMS condition.

rFEF-TMS selectively induces anterior-to-posterior global theta traveling waves

Based on our *a priori* hypothesis on anterior-to-posterior traveling waves, we specifically extracted traveling waves propagating from anterior to posterior direction across time and frequency. Despite the transient disruption of ongoing global traveling waves by TMS, stimulation of the rFEF led to a robust increase in anterior-to-posterior traveling wave activity in the theta frequency range (Fig. 5a; notice that this increase extends before TMS onset due to smearing from wavelet decomposition). In contrast, vertex stimulation produced a more confined increase in anterior-to-posterior wave activity that was largely restricted to the immediate post-TMS period (Fig. 5b). Comparison between conditions revealed a significant

cluster of enhanced anterior-to-posterior global theta traveling wave activity following rFEF stimulation, centered in the theta band (4.0–5.7 Hz) and spanning approximately 60–220 ms after stimulation (Fig. 5c; cluster-based permutation test, $p < 0.05$). Note that this effect was specific to the anterior-to-posterior axis, as analogous analyses along other directions (posterior-to-anterior, and both directions of the left-right and inferior-superior axes) did not reveal significant effects (see Supplementary Figs. S4 and S5). Together, these results demonstrate that TMS applied over the rFEF selectively induces theta-band traveling waves propagating along the anterior-to-posterior direction, presumably from the rFEF to occipital visual regions, beyond nonspecific effects of TMS on overall wave activity.

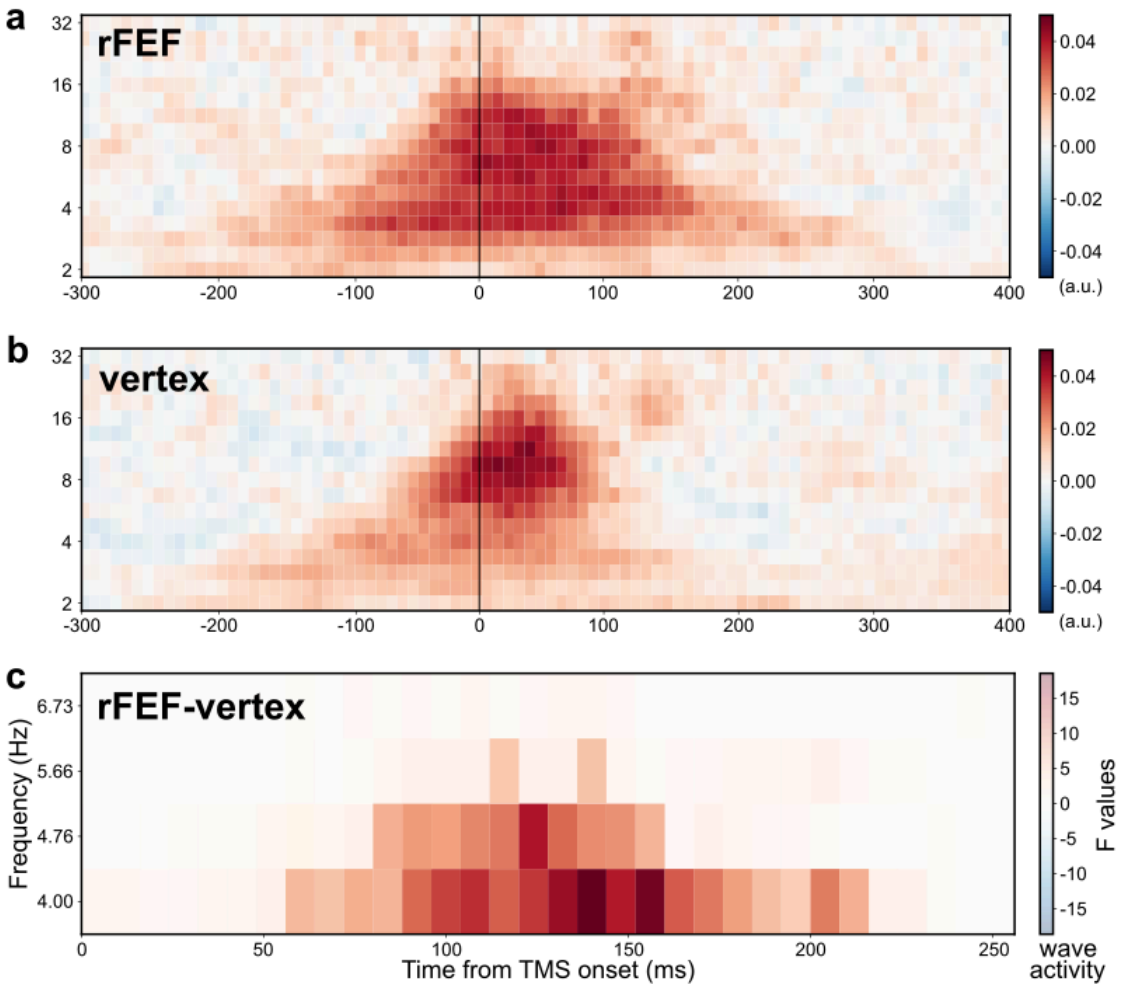

Fig. 5 rFEF-TMS selectively induces anterior-to-posterior global theta traveling waves. **a** Anterior-to-posterior traveling wave activity across time and frequency in the rFEF-TMS condition. The solid black line marks TMS onset (first pulse). **b** Same as **a**, but for the Vertex-TMS condition. **c** Differences in anterior-to-posterior traveling wave activity between rFEF-TMS and Vertex-TMS conditions, expressed in F values. Non-transparent regions indicate significant clusters identified by permutation testing.

rFEF-TMS modulates theta traveling waves rhythmically at 6.7 Hz

The behavioral data from this experiment were previously analyzed and reported in Dugué et al. (2019). This work demonstrated that TMS over the rFEF rhythmically modulates visual attentional search performance (measured as dprime) as a function of stimulation latency. Consistent with two-stage models of attention involving iterative communication between visual areas and higher-order regions, we then assessed whether global traveling waves support inter-areal communication in rhythmic attentional search. Specifically, we examined anterior-to-posterior global theta traveling waves as a function of TMS latency, and correlated TMS-induced wave activity with behavioral outcomes to assess the causal functional role of TMS-induced theta traveling waves in attentional search.

Wave activity was first averaged within the previously identified significant cluster between 60-220 ms (Fig. 5c) for each TMS latency and condition. Two-way repeated-measure analysis of variance (ANOVA) showed a significant main effect of TMS latency ($F(8) = 2.376$, $p = 0.021$), a significant main effect of TMS condition ($F(1) = 12.246$, $p = 0.003$), and a significant interaction between TMS latency and condition ($F(8) = 2.058$, $p = 0.045$). This result indicates that anterior-to-posterior global theta wave activity varies as a function of TMS latency, and that this effect is different between stimulations of the rFEF and the vertex.

We further examined the wave activity differences (rFEF-TMS minus Vertex-TMS) as a function of TMS latency (Fig. 6a). Spectral analysis using Fast Fourier Transform revealed a significant peak at 6.7 Hz, indicating that TMS-induced anterior-to-posterior global theta traveling waves are rhythmically modulated at this frequency (Fig. 6b). This modulation falls within the theta band and matches the periodicity previously reported for TMS effects on behavioral performance (Fig. 6a; note that more noise is expected in early latencies due to masking effects). Critically, the 6.7 Hz modulation was in phase across participants (Fig. 6b; Rayleigh test for circular data showed significant non-uniform distribution: $Z = 6.1$, $p = 0.001$).

Finally, we revealed a positive correlation between TMS-induced anterior-to-posterior global theta traveling waves and dprime modulation across individual participants and TMS latencies (Fig. 6c; Pearson's $r = 0.253$, $p = 0.002$).

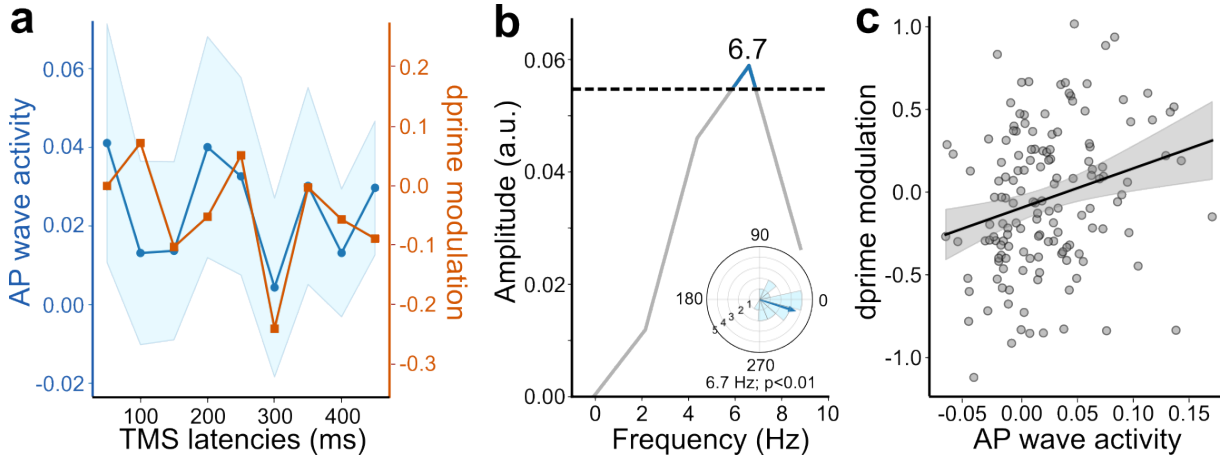

Fig. 6 rFEF-TMS modulates theta traveling waves rhythmically at 6.7 Hz. a Both anterior-to-posterior (AP) wave activity (blue lines) and dprime modulation (orange lines) are represented as a function of TMS latencies from the search array onset. Shaded area indicates 95% confidence interval. **b** Amplitude spectrum obtained from Fast Fourier Transform of averaged AP wave activity. Dashed line marks statistical threshold ($p = 0.05$) from permutation test. Polar histogram of individual participant phases (light bins) and their average (blue arrow) at the peak frequency (6.7 Hz). **c** Correlation between AP wave activity and dprime modulation across participants and latencies. The solid line indicates the linear regression fit, with shaded area representing the 95% confidence interval. A significant positive correlation was observed ($r = 0.253$, $p = 0.002$).

Discussion

This study investigated the causal functional role of global traveling waves in inter-areal communication during visual attention. By applying double-pulse TMS over the rFEF at multiple latencies in an attentional search task while recording EEG, we show that TMS pulses transiently interrupt ongoing global wave dynamics and selectively induce direction- and frequency-specific traveling waves. Critically, rFEF stimulation elicits anterior-to-posterior global theta traveling waves that are rhythmically modulated as a function of TMS latency during the task, consistent with rhythmic fluctuations in attentional search performance.

Cortical traveling waves have been linked to cognitive functions, including visual attention (for review Muller et al., 2018; Dugué & Chavane, 2025). Specifically, a recent EEG study observed that during the allocation of spatial attention, alpha-band traveling waves propagate more from

frontal to occipital electrodes than in the opposite direction along the same path (Alamia et al., 2023). To date, this remains the only study explicitly correlating visual attention with traveling waves. Recently, neural stimulation studies have demonstrated that external electrical perturbations can evoke or modulate propagating activity patterns in the cortex (Wei et al., 2024; Campbell et al., 2025). However, they have not established a causal link between traveling waves and cognition. Our results show that TMS can causally induce large-scale traveling waves that predict behavioral performance, providing direct evidence that traveling waves can have a causal functional role in attention.

Importantly, the traveling waves observed here are unlikely to reflect purely local activity generated at the stimulation site. Indeed, authors have raised concerns regarding the interpretability of apparent traveling waves observed in non-invasive recordings (for review Dugué & Chavane, 2025). A recent study analyzed the spatial-frequency spectrum of gray-matter activity in intra-cranial EEG recordings (a signal not subject to volume conduction) and demonstrated that low spatial frequencies dominate cortical dynamics (Alexander & Dugué, 2024). This argues against explanations based exclusively on localized sources or standing waves (Orsher et al., 2023; Zhigalov & Jensen, 2023). Instead, these results support the presence of large-scale traveling waves measurable at the scalp level, consistent with the present interpretation of global traveling waves coordinating inter-areal communication in visual attention.

Here, TMS was applied over the rFEF, which constrained the point of origin of the induced anterior-to-posterior traveling waves to that cortical region. The rFEF has long been shown to play a critical role in the attention network (for review Corbetta & Shulman, 2002; Corbetta et al., 2008) and be causally linked to endogenous attention (Fernandez et al., 2023). Stimulation of rFEF not only affects behavioral performance in visual attention tasks but also alters neural excitability and evoked responses in visual cortex (Taylor et al., 2007; Dugué et al., 2019; Veniero et al., 2021). This is consistent with other studies showing that the visual cortex is causally involved in such attentional tasks (Dugué et al., 2011; 2015). Although our analysis

pipeline does not directly determine the ending site of the traveling waves, the anterior-to-posterior propagation observed here suggests that TMS-induced traveling waves propagate toward occipital visual areas. Future studies will test this hypothesis by probing the endpoint of waves, for example by combining the present TMS-EEG approach with a second TMS coil targeting the visual cortex.

A key open question concerns the anatomical pathways underlying the non-invasively observed global traveling waves. The anterior-to-posterior propagation from rFEF to occipital cortex is consistent with the attention network (Corbetta & Shulman, 2002; Corbetta et al., 2008; Scolari et al., 2015), but the present data do not allow us to determine whether these waves propagate via direct cortico-cortical connections through intermediate regions (e.g., parietal cortex) or emerge from subcortical relays. In particular, the thalamus (e.g., pulvinar nucleus) interacts with rFEF and is thought to coordinate functional interactions across visual areas (Saalmann et al., 2012; Halassa & Kastner, 2017). Computational modeling studies further suggest that thalamo-cortical circuits can generate emergent traveling waves and shape their spatio-temporal properties (Alamia & VanRullen, 2019; Bhattacharya et al., 2021; Schwenk & Alamia, 2025). More generally, cortical traveling waves may be constrained by the structural connectome, whose topology shapes their propagation pathways, preferred directions, and frequencies (Koller et al., 2024). If propagation occurs through intermediate cortical regions, corresponding gradients of oscillatory power or phase shifts across the scalp would be expected. Future work using more spatially resolved approaches (likely in invasive recordings) as well as computational work (see Grabot et al., 2025) will be necessary to test these possibilities and directly characterize the underlying pathways of traveling waves.

Our findings are consistent with established theories of visual attention. Visual search has been postulated as a two-stage process involving low-level feature extraction and higher-order attentional selection, supported by iterative communication between visual areas and higher-order regions (Palmer et al., 1993; Treisman, 1998; Itti & Koch, 2001; Deco et al., 2002). Such exploratory behavior was more recently formalized in the rhythmic sampling theory of attention,

which proposes that attention explores the sensory environment rhythmically (for review VanRullen, 2016; Fiebelkorn & Kastner, 2019; Kienitz et al., 2022). Numerous studies have reported theta-band fluctuations in behavioral performance and neural oscillations during attention tasks (VanRullen et al., 2007; Landau & Fries, 2012; Fiebelkorn et al., 2013, 2018; Song et al., 2014; Chota et al., 2018; Helfrich et al., 2018; Senoussi et al., 2019; Michel et al., 2022; Galas et al., 2025). Our observation of functionally relevant traveling waves within the same frequency range provides strong empirical support that theta traveling waves are the underlying neural substrates of rhythmic attentional sampling.

Several influential theories have been proposed to explain the neural mechanisms underlying inter-areal communication, e.g., binding-by-synchrony (Singer & Gray, 1995), communication-through-coherence (Bastos et al., 2015), gating-by-inhibition (Jensen & Mazaheri, 2010), nested oscillations (Bonnefond et al., 2017). While these theories account for key temporal characteristics of oscillatory activity across brain regions, they generally conceptualize brain oscillations as stationary or locally synchronized processes. Instead, the traveling wave perspective considers temporal changes of global patterns of activity over areas of cortex, here large-scale cortex accessible via EEG. Our findings argue in favor of traveling waves supporting inter-areal communication, and are consistent with the latest proposal (Dugué & Chavane, 2025) that they constitute a canonical computation underlying diverse brain functions.

Methods

All data were originally collected as part of a previously published study, for which the behavioral results along with a detailed description of the experimental protocol have been published by Dugué et al. (2019). Here, we analyzed the EEG data and describe only the relevant materials and methods.

336 **Participants**

337 Twenty-three participants (7 women, age range: 24-38 years) with normal or corrected-to-
338 normal vision participated in the experiment. Two did not complete the experiment due to
339 discomfort during stimulation, and the EEG could not be recorded for five other participants for
340 technical reasons. The EEG data from 16 participants were included in the analysis. All
341 participants met the inclusion criteria for TMS and provided written informed consent prior to
342 participation. The study was conducted in accordance with the Declaration of Helsinki and was
343 approved by the local Ethics Committee (Sud-Ouest et Outre-Mer I; Protocol 2009-A01087-
344 50).

345 **Visual Search Task**

346 Participants performed an attentional visual search task (Fig. 1a; same procedure as in Dugué
347 et al., 2011; Dugué et al., 2015). Visual stimuli were displayed on a screen (36.5 × 27 degree
348 of visual angle, °VA) positioned 57 cm from the participant in a dark room. On each trial, four
349 stimuli of identical size (1.5 × 1.5°VA) were presented at a fixed eccentricity (6°VA) in the left
350 visual field. The stimulus array consisted either of four distractors ('L's; target absent trials) or
351 of three distractors and one target randomly in one of the four stimulus locations ('T'; target
352 present trials). All items were randomly oriented (0, 90, 180, or 270° from upright).

353 After an individually determined stimulus-onset asynchrony (one-up-two-down staircase) to
354 achieve approximately 70% correct performance (mean ± standard deviation: 85 ± 8 ms), the
355 search array was masked, such that the total duration of visual stimulation was 500 ms.
356 Participants were instructed to report the absence or presence of target 'T' by key press, with
357 an emphasis on accuracy and no time pressure. The intertrial interval was jittered between
358 1000 and 2000 ms to minimize cumulative effects of stimulation. Participants completed 26
359 blocks of 72 trials each, including one practice block, one staircase block, four blocks without
360 TMS, ten blocks with TMS applied over the rFEF (rFEF-TMS) and ten control blocks with TMS

361 applied over the vertex (Vertex-TMS). The present study focuses the analyses on the rFEF-
362 TMS and Vertex-TMS blocks.

363 **TMS procedure**

364 TMS pulses were delivered using a Magstim Rapid^2 stimulator (biphasic; Magstim Company,
365 Whitland, UK) equipped with a 70-mm figure-of-eight coil. Stimulation was remotely triggered
366 via Matlab R2014 from the stimulus presentation computer (Mathworks Inc., Natick, MA).
367 Stimulation intensity was initially set at 50% of maximal output and individually adjusted to just
368 below the threshold for facial and temporal muscle activation (mean ± standard error to the
369 mean: 52 ± 2%). The coil was positioned tangentially to the scalp, with its handle oriented
370 about 45° backward and laterally.

371 The stimulation target over the rFEF was defined based on averaged Talairach coordinates (x
372 = 31, y = −2, z = 47). For 11 participants, coil positioning was guided by individual T1-weighted
373 anatomical MRIs (3T Philips) using these coordinates. For the remaining participants, for
374 whom anatomical MRI scans were not available, the stimulation site was defined as the
375 barycenter (between electrodes F2 and FC4) of the rFEF locations identified in the MRI-guided
376 participants. To control for nonspecific TMS effects (e.g., clicking noise and tapping sensation),
377 TMS was also applied over the vertex as the control condition (block-designed,
378 counterbalanced), which was individually defined as the location of electrode Cz (O'Shea et
379 al., 2004). The vertex has been commonly used as an active control site for TMS studies, as
380 it has minimal involvement in task-related processes (Jung et al., 2016).

381 Double-pulse TMS (inter-pulse interval: 25 ms) was delivered at one of nine possible latencies
382 relative to search array onset (50-450 ms, in 50-ms increments). Double-pulse TMS was used
383 instead of single-pulse stimulation because paired pulses have been shown to produce
384 stronger and more reliable behavioral effects, particularly in visual search (Juan & Walsh,
385 2003; Kalla et al., 2008; Dugué et al., 2011, 2015; Yan et al., 2016).

386 **EEG recording and pre-processing**

387 EEG data were recorded using a TMS-compatible 64-channel EEG cap (standard antiCAP
388 snap; 10–20 system; EasyCap GmbH, Herrsching, Germany). Electrodes Fpz and FCz served
389 as ground and reference, respectively. Signals were sampled at 5000 Hz and acquired with an
390 online low-pass filter at 1000 Hz.

391 EEG data were preprocessed using custom scripts in combination with the MNE-Python
392 toolbox (Gramfort et al., 2013), following recommendations from TMS-EEG Signal Analyzer's
393 pipeline for TMS-EEG analysis (Rogasch et al., 2017). TMS-related artifacts in the raw EEG
394 time series were removed (-1 to 15 ms relative to each pulse) and replaced using cubic
395 interpolation based on five samples (1 ms) on each side of the interpolated window. Bad
396 channels were identified by visual inspection and interpolated using MNE-Python's spline
397 interpolation. Data were then lowpass filtered at 330 Hz (finite impulse response, FIR;
398 Hamming window; zero-phase; 82.5 Hz transition bandwidth; 53 dB stopband attenuation;
399 passband edge 330 Hz; cutoff frequency 371.25 Hz; filter length 0.040 s) before being down-
400 sampled to 1000 Hz to avoid aliasing.

401 Continuous data were epoched from -2 to 5 s relative to search array onset, followed by manual
402 rejection of bad epochs. To remove large-amplitude artifacts (e.g., TMS-evoked muscle
403 artifacts), independent component analysis (FastICA, 15 components) was performed on
404 concatenated runs separately for rFEF-TMS and Vertex-TMS conditions. Cubic interpolation
405 around TMS pulses was then applied again using the same parameters. After high-pass
406 filtering at 0.1 Hz (FIR; Hamming window; minimum non-linear phase; 0.10 Hz transition
407 bandwidth; 53 dB stopband attenuation), a second FastICA was performed to remove residual
408 artifacts (e.g., blinks, eye movements, and muscle activity). Cubic interpolation around TMS
409 pulses was subsequently applied once more.

410 Finally, EEG data were re-referenced to the common average. Channels TP9, TP10 and Iz
411 were excluded due to their too-far distance from the remaining electrodes for the spatial phase
412 unwrapping (see Traveling Waves Analysis section) leaving a total of 59 electrodes for the
413 analysis. To equalize trial counts across conditions and participants, analyses were restricted
414 to the first 400 trials for each of the rFEF-TMS and Vertex-TMS conditions.

415 **Time frequency decomposition**

416 Time-frequency representations were computed using Morlet wavelet convolution. Phase and
417 amplitude were estimated using two-cycle Morlet wavelets at 17 logarithmically spaced center
418 frequencies ranging from 2 to 32 Hz. To reduce computational load, the resulting time-series
419 of phase and power were down-sampled by a factor of eight resulting in a sampling rate of 125
420 Hz.

421 Grand-average power was first computed by averaging across all 59 electrodes and trials.
422 Power values were then normalized into decibels relative to a pre-stimulus baseline (−1000 to
423 −600 ms from search array onset). Significant clusters of induced power against baseline
424 activity were identified using a cluster-based permutation test (Maris & Oostenveld, 2007; 5000
425 permutations, two-tailed), with a cluster-forming threshold of p = 0.001 and a cluster-level
426 significance threshold of p = 0.05. Differences in induced power between the rFEF-TMS and
427 Vertex-TMS conditions were assessed using cluster-based permutation test (Maris &
428 Oostenveld, 2007; 5000 permutations, two-tailed, cluster-level p = 0.05).

429 Topographic maps of induced power (decibel-normalized) were computed by averaging power
430 within selected time-frequency windows defined from the grand-average data. Peak
431 frequencies were identified from power spectra averaged across time, and for each frequency,
432 a 100-ms time window centered on the peak latency was selected (outlined in Fig. 2a and 2b).
433 After within-participant topographic normalization, significant power increase was identified

using threshold-free cluster enhancement permutation tests (5000 permutations, one-tailed, $p = 0.05$).

Traveling Wave Analysis

Cortical traveling waves were analyzed in single-trial EEG data using an SVD-based approach (Alexander et al., 2013). Complex-valued phase estimates (Φ) obtained from wavelet convolution were first converted, at each sample (time × frequency × trial × sensor), into real-valued relative phases (Ψ, relative to an arbitrary electrode) by computing nearest-neighbor phase differences across the electrode array and then reintegrating these differences in radians (spatial phase unwrapping; Fig. 1c). Specifically, for neighboring electrodes *i* and *j* (determined by Delaunay triangulation), their phase difference was defined as:

$$\Delta\theta_{ij} = \arg(\Phi_i) - \arg(\Phi_j) + 2\pi k_{ij},\ k_{ij} \in Z, \qquad (1)$$

with integer k_{ij} chosen such that $\Delta\theta_{ij} \in [-\pi, \pi)$. The relative phase at each electrode was then reconstructed by cumulatively adding these nearest-neighbor differences ($\Delta\theta$) according to:

$$\Psi i = \Psi j + \Delta\theta_{ij} \quad (2)$$

starting from an arbitrary reference electrode. These nearest-neighbor phase differences were sequentially integrated into an initially edgeless graph, in ascending order of $|\Delta\theta_{ij}|$. When the condition $|\Delta\theta_{ij}| << \pi$ is not satisfied everywhere, inconsistencies may arise such that $\Psi i - \Psi j = \delta\Phi ij + 2k\pi$ for some integer $k \neq 0$. In data where phase varies smoothly across electrodes, the number of such inconsistencies is small relative to the total number of nearest neighbors. These inconsistencies may reflect either genuine phase discontinuities or measurement noise (Spagnolini, 1995). Integrating phase differences by increasing $|\Delta\theta_{ij}|$ preferentially localizes such errors to regions exhibiting the largest phase differences, corresponding to legitimate discontinuities or elevated noise.

At the single-participant level, SVD was applied to the relative phase data to reduce dimensionality and extract dominant spatial patterns of phase dynamics across the scalp. For each participant, relative phase values were arranged into a matrix $A \in R^{Ne \times Ns}$, where N_e denotes the number of electrodes and N_s the number of samples collapsed across time, frequency, trial, and TMS condition. The matrix A was decomposed by SVD as

$$A = U\Sigma V^T, \qquad (3)$$

where U contains the left singular vectors (LSVs), Σ is a diagonal matrix of singular values σ_r ordered in descending magnitude, and V contains the right singular vectors. The LSVs represent orthogonal spatial basis vectors that capture dominant phase gradients across the electrode array, whereas the corresponding singular values (σ) quantify the square root of the variance explained by each vector. By definition, these empirically-derived vectors are orthogonal and can be treated as independent modes of the system; thus, weighted linear combinations of the LSVs can recover the original phase data without loss.

Spatial basis vectors were retained in descending order of explained variance, with the first three to four components typically corresponding to a spatial frequency of approximately one cycle across the electrode array. These participant-specific spatial basis vectors represent global traveling wave components, each corresponding to an orthogonal direction of phase propagation across the scalp. Linear combinations of these spatial basis vectors reconstitute all possible global TW components.

To facilitate interpretation and comparison across participants, the individual spatial basis vectors were projected onto a common set of axes defined by electrode coordinates in three Cartesian dimensions (anterior-posterior, inferior-superior, and left-right; Fig. 3a). This procedure effectively rotates each individual's spatial basis vectors to a shared cardinal reference frame, enabling direct cross-participant comparison. Prior to projection, phase values were normalized according to:

$$C_{norm} = (C_{x,y,z} - \min(C_{x,y,z})) / (\max(C_{x,y,z}) - \min(C_{x,y,z})) * R_{mean}, \quad (4)$$

where $C_{x,y,z}$ denotes the phase values expressed in electrode coordinate space and R_{mean} defines the mean range of the retained spatial basis vectors. Projection coefficients were then computed as

$$\beta = U_R^T C_{norm}, \quad (5)$$

where U_R contains the first *R* spatial basis vectors obtained from SVD, with R determined by the number of global traveling wave components retained (here *R* = 4). Reconstructed phase dynamics were obtained as:

$$C_{rec} = U_R \beta, \quad (6)$$

yielding sample-by-sample estimates of wave activity, aggregated across all bases (global wave activity; Fig. 4) or, for direction-specific measures restricted to individual cardinal bases (e.g., anterior-to-posterior waves; Fig. 5).

Single-trial global wave activity was re-aligned to TMS onset and averaged across trials, followed by baseline correction using a pre-TMS interval (−1000 to −600 ms). For each condition, significant modulations of wave activity were assessed using two-tailed cluster-based permutation tests (Maris & Oostenveld, 2007; 5000 permutations), with a cluster-forming threshold of $p = 0.001$ and a cluster-level significance threshold of $p = 0.05$.

TMS-related anterior-to-posterior wave activity was then compared between the rFEF-TMS and Vertex-TMS conditions using cluster-based permutation testing (Maris & Oostenveld, 2007; 5000 permutations, two-tailed, $p = 0.05$). Statistical testing was restricted to a pre-defined time-frequency window (4-7 Hz, 0-250 ms relative to TMS onset). The theta frequency band was selected based on the *a priori* hypothesis that theta traveling waves have a causal functional role in attentional search; the temporal window was chosen based on previous time-frequency analyses showing maximal grand-average power in this interval (Fig. 2a and 2b).

To characterize the rhythmic modulation of TMS on anterior-to-posterior global theta traveling waves, wave activity was averaged within the significant cluster identified above, and differences between rFEF-TMS and Vertex-TMS conditions were computed as a function of TMS latency. Periodicity was assessed by applying a Fast Fourier Fransform to the detrended time series (Kienitz et al., 2022). Statistical significance at each frequency was evaluated using a bootstrapping procedure. Specifically, TMS latency labels were randomly permuted within participants (100,000 iterations). For each surrogate spectrum, the maximum amplitude across frequencies was retained to correct for multiple comparisons. The empirical spectrum was considered significant if it exceeded the 95th percentile of the surrogate distribution ($p < 0.05$). For the frequency showing a significant amplitude peak, phase values were extracted for each participant to verify that the observed periodicity was in phase across participants, and the circular distribution of these phases was assessed using a Rayleigh test for non-uniformity. Finally, Pearson correlation coefficients were computed to assess the link between anterior-to-posterior waves and dprime modulation across participants and latencies. Although wave activity was quantified at the single-trial level, behavioral performance was better summarized using dprime, a sensitivity measure free of decision biases (Green & Swets, 1966) that inherently requires trial aggregation. This metric isolates perceptual sensitivity from response bias and therefore constitutes a more reliable and theoretically appropriate measure for relating neural dynamics to behavior.

Acknowledgements

This project has received funding from the European Research Council (ERC) under the European Union's Horizon 2020 research and innovation programme (grant agreement No 852139 - Laura Dugué). We also thank Alexy-Assaf Beck for collecting the data for the original experiment (Dugué et al., 2019), as well as Andrea Alamia and Camille Fakche for their useful comments on the manuscript.

Author contributions

L.D. and Y.K. designed the research. Y.K. and D.M.A. performed the analysis of the data. Y.K., D.M.A. and L.D. interpreted the data. Y.K. wrote the first version of the manuscript. All authors revised and edited subsequent versions of the manuscript.

Declaration of interests

The authors declare no competing interests.

Data and code availability

All data and analysis code will be made publicly available upon acceptance of the manuscript. The MEG_Chicken toolbox (https://github.com/DugueLab/MEG_Chicken) was used by the first author as a training program for artifact detection (combined with training from the senior authors).

References

Alamia, A., Terral, L., D'ambra, M. R., & VanRullen, R. (2023). Distinct roles of forward and backward alpha-band waves in spatial visual attention. *eLife*, *12*, e85035.

Alamia, A., & VanRullen, R. (2019). Alpha oscillations and traveling waves: Signatures of predictive coding?. *PLoS Biology*, *17*(10), e3000487.

Alexander, D. M., & Dugué, L. (2024). The dominance of large-scale phase dynamics in human cortex, from delta to gamma. *ELife*, *13*, RP100674.

Alexander, D. M., Jurica, P., Trengove, C., Nikolaev, A. R., Gepshtein, S., Zvyagintsev, M., ... & van Leeuwen, C. (2013). Traveling waves and trial averaging: the nature of single-trial and averaged brain responses in large-scale cortical signals. *Neuroimage*, *73*, 95-112.

Bastos, A. M., Vezoli, J., & Fries, P. (2015). Communication through coherence with inter-areal delays. *Current opinion in neurobiology*, *31*, 173-180.

Bonnefond, M., Kastner, S., & Jensen, O. (2017). Communication between brain areas based on nested oscillations. *eneuro*, *4*(2).

Bhattacharya, S., Cauchois, M. B., Iglesias, P. A., & Chen, Z. S. (2021). The impact of a closed-loop thalamocortical model on the spatiotemporal dynamics of cortical and thalamic traveling waves. *Scientific reports*, *11*(1), 14359.

Campbell, J. M., Davis, T. S., Anderson, D. N., Arain, A., Davis, Z. W., Inman, C. S., ... & Rolston, J. D. (2025). Macroscale traveling waves evoked by single-pulse stimulation of the human brain. *Journal of Neuroscience*, *45*(21).

Chota, S., Luo, C., Crouzet, S. M., Boyer, L., Kienitz, R., Schmid, M. C., & VanRullen, R. (2018). Rhythmic fluctuations of saccadic reaction time arising from visual competition. *Scientific reports*, *8*(1), 15889.

Corbetta, M., Patel, G., & Shulman, G. L. (2008). The reorienting system of the human brain: from environment to theory of mind. *Neuron*, *58*(3), 306-324.

Corbetta, M., & Shulman, G. L. (2002). Control of goal-directed and stimulus-driven attention in the brain. *Nature reviews neuroscience*, *3*(3), 201-215.

Davis, Z. W., Muller, L., Martinez-Trujillo, J., Sejnowski, T., & Reynolds, J. H. (2020). Spontaneous travelling cortical waves gate perception in behaving primates. *Nature*, *587*(7834), 432-436.

Deco, G., Pollatos, O., & Zihl, J. (2002). The time course of selective visual attention: theory and experiments. *Vision research*, *42*(27), 2925-2945.

Dugué, L., Beck, A. A., Marque, P., & VanRullen, R. (2019). Contribution of FEF to attentional periodicity during visual search: A TMS study. *Eneuro*, *6*(3).

Dugué, L., & Chavane, F. (2025). Traveling waves across scales: Different mechanisms but same canonical computation? *ELife*, *14*, e106753.

Dugué, L., Marque, P., & VanRullen, R. (2011). Transcranial magnetic stimulation reveals attentional feedback to area V1 during serial visual search. *PLoS One*, *6*(5), e19712.

Dugué, L., Marque, P., & VanRullen, R. (2015). Theta oscillations modulate attentional search performance periodically. *Journal of cognitive neuroscience*, *27*(5), 945-958.

Dugué, L., & VanRullen, R. (2017). Transcranial magnetic stimulation reveals intrinsic perceptual and attentional rhythms. *Frontiers in Neuroscience*, *11*, 154.

Fakche, C., & Dugué, L. (2024). Perceptual Cycles Travel Across Retinotopic Space. *Journal of Cognitive Neuroscience*, *36*(1), 200–216.

Fakche, C., Galas, L., Petras, K., & Dugué, L. (2024). Alpha traveling waves index spatial attention. *Journal of Vision*, *24*(10), 530-530.

Fernández, A., Hanning, N. M., & Carrasco, M. (2023). Transcranial magnetic stimulation to frontal but not occipital cortex disrupts endogenous attention. *Proceedings of the national academy of sciences*, *120*(10), e2219635120.

Fiebelkorn, I. C., & Kastner, S. (2019). A Rhythmic Theory of Attention. *Trends in Cognitive Sciences*, *23*(2), 87–101.

Fiebelkorn, I. C., Pinsk, M. A., & Kastner, S. (2018). A dynamic interplay within the frontoparietal network underlies rhythmic spatial attention. *Neuron*, *99*(4), 842-853.

Fiebelkorn, I. C., Saalmann, Y. B., & Kastner, S. (2013). Rhythmic sampling within and between objects despite sustained attention at a cued location. *Current biology*, *23*(24), 2553-2558.

Galas, L., Donovan, I., & Dugué, L. (2025). Attention rhythmically shapes sensory tuning. *Journal of Neuroscience*, *45*(7), e1616242024.

Grabot, L., Merholz, G., Winawer, J., Heeger, D. J., & Dugué, L. (2025). Traveling waves in the human visual cortex: An MEG-EEG model-based approach. *PLOS Computational Biology*, *21*(4), e1013007.

Gramfort, A., Luessi, M., Larson, E., Engemann, D. A., Strohmeier, D., Brodbeck, C., ... & Hämäläinen, M. (2013). MEG and EEG data analysis with MNE-Python. *Frontiers in Neuroinformatics*, *7*, 267.

Green, D. M., & Swets, J. A. (1966). *Signal detection theory and psychophysics* (Vol. 1, pp. 1969-2012). New York: Wiley.

Halassa, M. M., & Kastner, S. (2017). Thalamic functions in distributed cognitive control. *Nature neuroscience*, *20*(12), 1669-1679.

Helfrich, R. F., Fiebelkorn, I. C., Szczepanski, S. M., Lin, J. J., Parvizi, J., Knight, R. T., & Kastner, S. (2018). Neural mechanisms of sustained attention are rhythmic. *Neuron*, *99*(4), 854-865.

Itti, L., & Koch, C. (2001). Computational modelling of visual attention. *Nature reviews neuroscience*, *2*(3), 194-203.

Jensen, O., & Mazaheri, A. (2010). Shaping functional architecture by oscillatory alpha activity: gating by inhibition. *Frontiers in human neuroscience*, *4*, 186.

Juan, C. H., & Walsh, V. (2003). Feedback to V1: a reverse hierarchy in vision. *Experimental brain research*, *150*(2), 259-263.

Jung, J., Bungert, A., Bowtell, R., & Jackson, S. R. (2016). Vertex stimulation as a control site for transcranial magnetic stimulation: a concurrent TMS/fMRI study. *Brain stimulation*, *9*(1), 58-64.

Kalla, R., Muggleton, N. G., Juan, C. H., Cowey, A., & Walsh, V. (2008). The timing of the involvement of the frontal eye fields and posterior parietal cortex in visual search. *Neuroreport*, *19*(10), 1067-1071.

Kienitz, R., Schmid, M. C., & Dugué, L. (2022). Rhythmic sampling revisited: Experimental paradigms and neural mechanisms. *European Journal of Neuroscience*, *55*(11-12), 3010-3024.

Koller, D. P., Schirner, M., & Ritter, P. (2024). Human connectome topology directs cortical traveling waves and shapes frequency gradients. *Nature Communications*, *15*(1), 3570.

Landau, A. N., & Fries, P. (2012). Attention Samples Stimuli Rhythmically. *Current Biology*, *22*(11), 1000–1004.

Landau, A. N., Schreyer, H. M., Van Pelt, S., & Fries, P. (2015). Distributed attention is implemented through theta-rhythmic gamma modulation. *Current biology*, *25*(17), 2332-2337.

Lozano-Soldevilla, D., & VanRullen, R. (2019). The Hidden Spatial Dimension of Alpha: 10-Hz Perceptual Echoes Propagate as Periodic Traveling Waves in the Human Brain. *Cell Reports*, *26*(2), 374-380.e4.

Maris, E., & Oostenveld, R. (2007). Nonparametric statistical testing of EEG-and MEG-data. *Journal of neuroscience methods*, *164*(1), 177-190.

Michel, R., Dugué, L., & Busch, N. A. (2022). Distinct contributions of alpha and theta rhythms to perceptual and attentional sampling. *European Journal of Neuroscience*, *55*(11-12), 3025-3039.

Muller, L., Chavane, F., Reynolds, J., & Sejnowski, T. J. (2018). Cortical travelling waves: mechanisms and computational principles. *Nature Reviews Neuroscience*, *19*(5), 255-268.

Orsher, Y., Rom, A., Perel, R., Lahini, Y., Blinder, P., & Shein-Idelson, M. (2023). Travelling waves or sequentially activated discrete modules: mapping the granularity of cortical propagation. *ELife, 12*, RP92254.

O'shea, J., Muggleton, N. G., Cowey, A., & Walsh, V. (2004). Timing of target discrimination in human frontal eye fields. *Journal of Cognitive Neuroscience*, *16*(6), 1060-1067.

Palmer, J., Ames, C. T., & Lindsey, D. T. (1993). Measuring the effect of attention on simple visual search. *Journal of Experimental Psychology: Human Perception and Performance*, *19*(1), 108.

Petras, K., Grabot, L., & Dugué, L. (2025). Locally induced traveling waves generate globally observable traveling waves. *Journal of Neuroscience*, *45*(34).

Plöchl, M., Fiebelkorn, I., Kastner, S., & Obleser, J. (2022). Attentional sampling of visual and auditory objects is captured by theta-modulated neural activity. *European Journal of Neuroscience*, *55*(11-12), 3067-3082.

Rogasch, N. C., Sullivan, C., Thomson, R. H., Rose, N. S., Bailey, N. W., Fitzgerald, P. B., ... & Hernandez-Pavon, J. C. (2017). Analysing concurrent transcranial magnetic stimulation and electroencephalographic data: A review and introduction to the open-source TESA software. *Neuroimage*, *147*, 934-951.

Saalmann, Y. B., Pinsk, M. A., Wang, L., Li, X., & Kastner, S. (2012). The pulvinar regulates information transmission between cortical areas based on attention demands. *science*, *337*(6095), 753-756.

Scolari, M., Seidl-Rathkopf, K. N., & Kastner, S. (2015). Functions of the human frontoparietal attention network: Evidence from neuroimaging. *Current opinion in behavioral sciences*, *1*, 32-39.

Schwenk, J. C., & Alamia, A. (2025). A hierarchical multiscale model of forward and backward alpha-band traveling waves in the visual system. *PLOS Computational Biology*, *21*(8), e1013294.

Senoussi, M., Moreland, J. C., Busch, N. A., & Dugué, L. (2019). Attention explores space periodically at the theta frequency. *Journal of vision*, *19*(5), 22-22.

Singer, W., & Gray, C. M. (1995). Visual feature integration and the temporal correlation hypothesis. *Annual review of neuroscience*, *18*(1), 555-586.

Song, K., Meng, M., Chen, L., Zhou, K., & Luo, H. (2014). Behavioral oscillations in attention: rhythmic α pulses mediated through θ band. *Journal of Neuroscience*, *34*(14), 4837-4844.

Spagnolini, U. (1995). 2-D phase unwrapping and instantaneous frequency estimation. *IEEE Transactions on Geoscience and Remote Sensing*, *33*(3), 579-589.

Taylor, P. C., Nobre, A. C., & Rushworth, M. F. (2007). FEF TMS affects visual cortical activity. *Cerebral cortex*, *17*(2), 391-399.

Treisman, A. (1998). Feature binding, attention and object perception. *Philosophical Transactions of the Royal Society of London. Series B: Biological Sciences*, *353*(1373), 1295-1306.

VanRullen, R. (2016). Perceptual cycles. *Trends in cognitive sciences*, *20*(10), 723-735.

VanRullen, R., Carlson, T., & Cavanagh, P. (2007). The blinking spotlight of attention. *Proceedings of the National Academy of Sciences*, *104*(49), 19204-19209.

Veniero, D., Gross, J., Morand, S., Duecker, F., Sack, A. T., & Thut, G. (2021). Top-down control of visual cortex by the frontal eye fields through oscillatory realignment. *Nature communications*, *12*(1), 1757.

Wei, J., Alamia, A., Yao, Z., Huang, G., Li, L., Liang, Z., ... & Zhang, Z. (2024). State-dependent tACS effects reveal the potential causal role of prestimulus alpha traveling waves in visual contrast detection. *Journal of Neuroscience*, *44*(27).

Yan, Y., Wei, R., Zhang, Q., Jin, Z., & Li, L. (2016). Differential roles of the dorsal prefrontal and posterior parietal cortices in visual search: a TMS study. *Scientific reports*, *6*(1), 30300.

Zhang, H., Watrous, A. J., Patel, A., & Jacobs, J. (2018). Theta and Alpha Oscillations Are Traveling Waves in the Human Neocortex. *Neuron*, *98*(6), 1269-1281.e4. Q1.

Zhigalov, A., & Jensen, O. (2023). Perceptual echoes as travelling waves may arise from two discrete neuronal sources. *NeuroImage*, *272*, 120047.

Supplementary Information

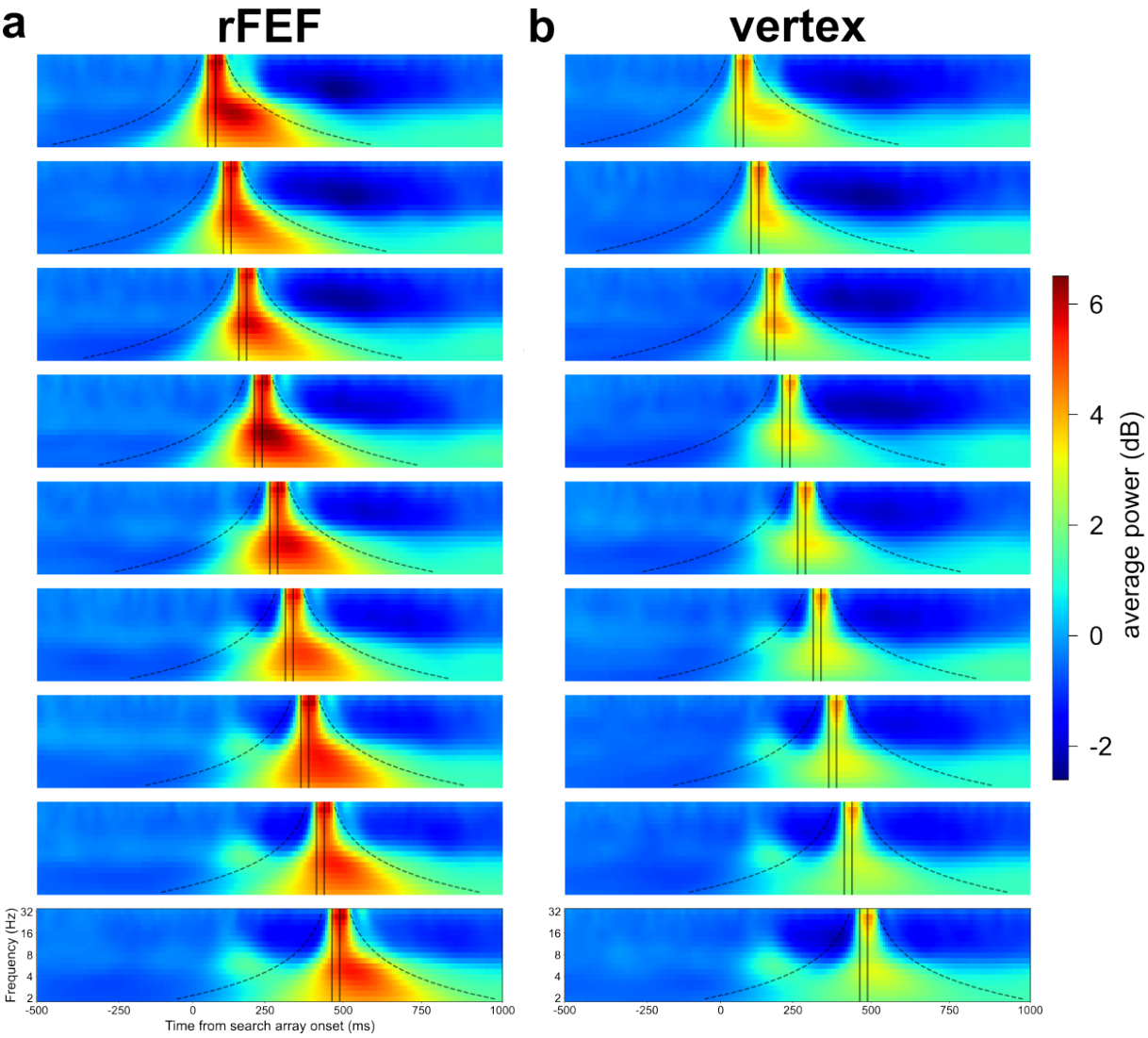

Supplementary Fig. S1 TMS-induced power systematically shifts across TMS latencies. **a** Grand-average time-frequency power (across participants, trials and sensors) in the rFEF-TMS condition. The solid black lines indicate single-pulse TMS onsets. The cone of influence is overlayed (area potentially impacted by artifactual spread of the TMS-induced activity). Only the TMS-induced activity exhibited systematic temporal shifts across TMS latencies, whereas visually-induced theta power (around 100-200ms) remained stable in both timing and magnitude across TMS latencies and stimulation conditions. **b** Same as **a**, but for the Vertex-TMS (control) condition.

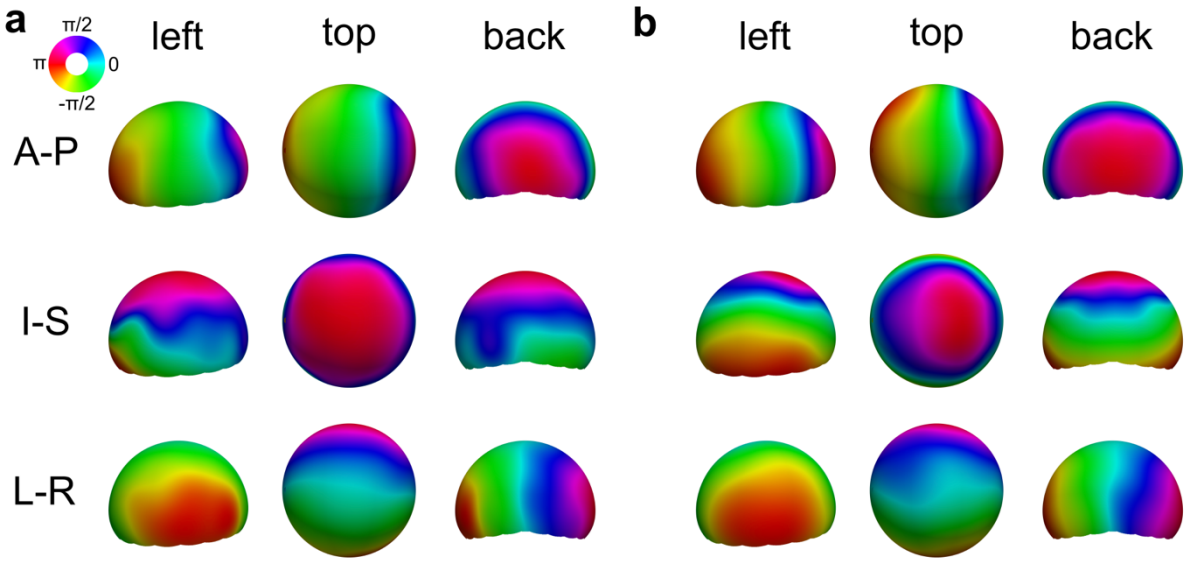

Supplementary Fig. S2 Global traveling waves components for two example participants. a Global traveling wave components projected onto cardinal axes for an example participant. A-P: anterior-posterior; I-S: inferior-superior; L-R: left-right. **b** Same as **a**, for another example participant.

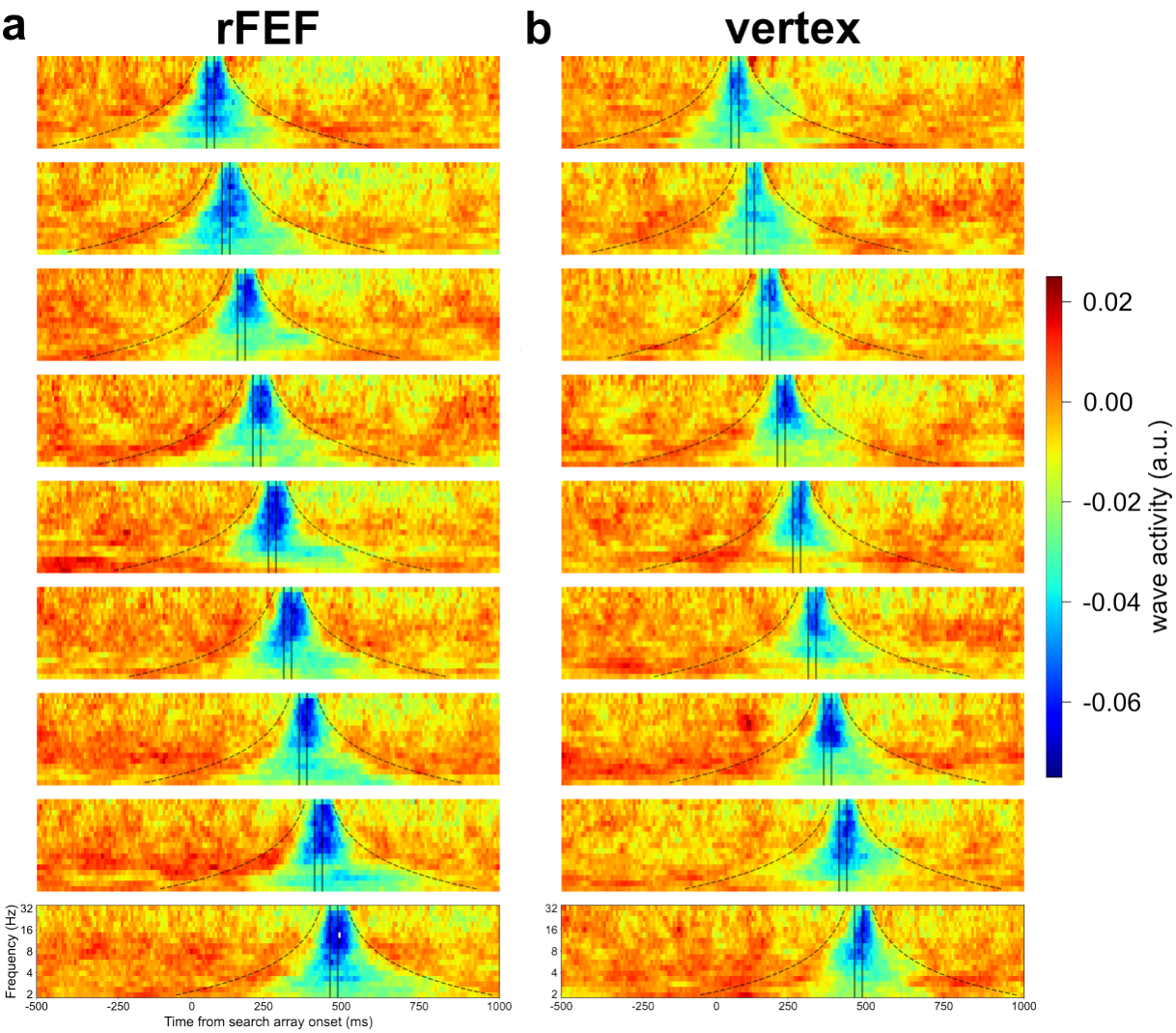

Supplementary Fig. S3 Disruption of global wave activity shifts across TMS latencies. a Global traveling wave activity across time and frequency in the rFEF-TMS condition. The solid black lines mark TMS pulse onsets. The cone of influence is overlayed. TMS transiently disrupts global wave activity, and this disruption is temporally specific to the TMS pulses, as evidenced by its systematic temporal shift across different TMS latencies. **b** Same as **a**, but for the Vertex-TMS condition.

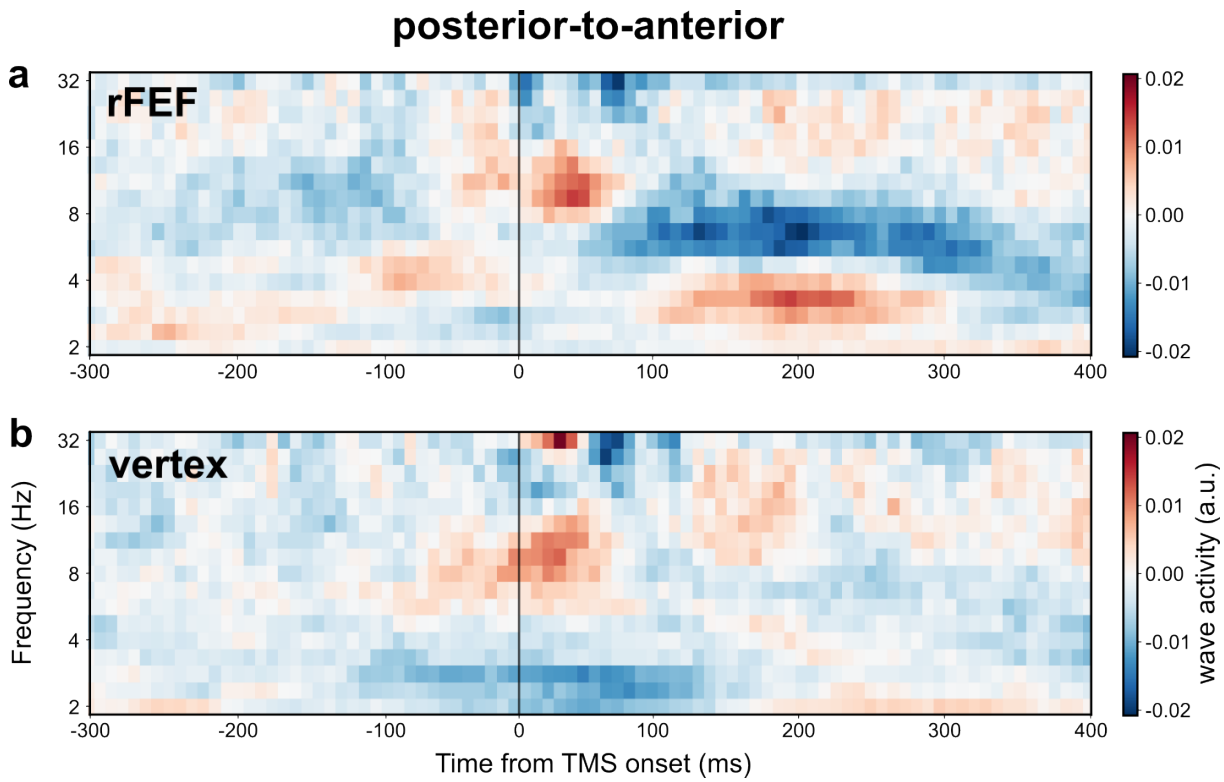

Supplementary Fig. S4 Posterior-to-anterior traveling wave activity following TMS. a Posterior-to-anterior traveling wave activity across time and frequency in the rFEF-TMS condition. The solid black line marks TMS onset (first pulse). **b** Same as **a**, but for the Vertex-TMS condition. In contrast to the anterior-to-posterior direction, no significant clusters were observed in the theta band for the posterior-to-anterior direction.

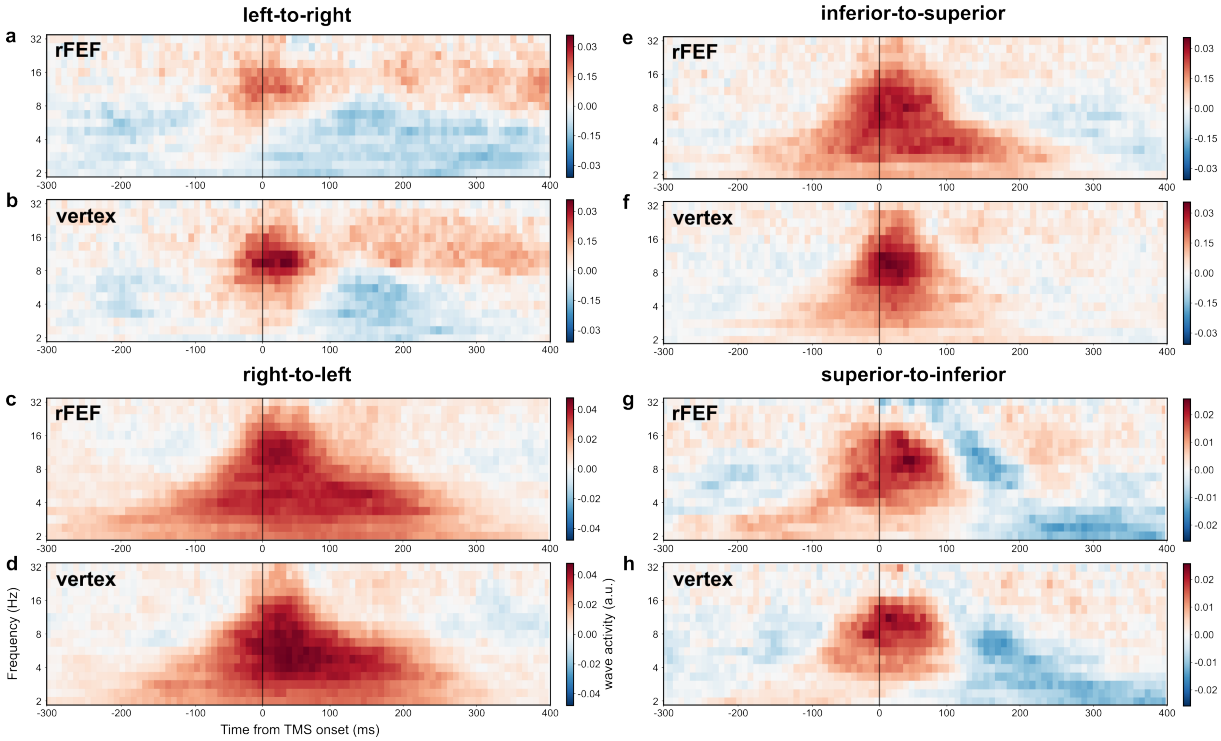

Supplementary Fig. S5 Traveling wave activity along other Cartesian axes following TMS. **a** Left-to-right traveling wave activity across time and frequency in the rFEF-TMS condition. The solid black line marks TMS onset (first pulse). **b** Same as **a**, but for the Vertex-TMS condition. **c** Right-to-left traveling wave activity across time and frequency in the rFEF-TMS condition. **d** Same as **c**, but for the Vertex-TMS condition. **e** Inferior-to-superior traveling wave activity across time and frequency in the rFEF-TMS condition. **f** Same as **e**, but for the Vertex-TMS condition. **g** Superior-to-inferior traveling wave activity across time and frequency in the rFEF-TMS condition. **h** Same as **g**, but for the Vertex-TMS condition. None of these Cartesian directions exhibited significant cluster-level difference in theta traveling waves between rFEF-TMS and Vertex-TMS conditions.